IEEE Access
Multidisciplinary | Rapid Review | Open Access Journal

Received 25 December 2022, accepted 9 January 2023, date of publication 13 January 2023, date of current version 7 February 2023.

Digital Object Identifier 10.1109/ACCESS.2023.3236815

RESEARCH ARTICLE

A Compact and Coupling-Smooth Magnetic Coupler Design for AGV Wireless Charging Application

CHAOWEI FU, (Member, IEEE), DEYU WANG, (Member, IEEE), AND QINGLIN ZHAO
School of Electrical Engineering, Yanshan University, Qinhuangdao 066000, China

Corresponding author: Deyu Wang (wdy@ysu.edu.cn)

This work was supported by the Key Project of Science and Technology Program of Colleges and Universities of Education Department of Hebei Province under Grant ZD2021101.

ABSTRACT A compact magnetic coupler of inductive power transfer (IPT) system for automated guided vehicles (AGVs) is proposed in this paper, which consists of a double-D (DD) transmitter (Tx) and a compact dual-coil receiver (Rx). By overlapping between one coupling peak point and another coupling null point of two Rx coils, the Rx of the magnetic coupler achieves relatively small output voltage fluctuations, as well as minimizes its size. In addition, to eliminate cross-coupling of the dual-coil Rx, a mutual decoupling device composed of two lumped inductors is adopted, which possesses the same mutual inductance as the dual-coil Rx. Finally, based on the proposed magnetic coupler and its unique way of decoupling, a 3kW IPT system is constructed with 180mm×390mm Tx, 150mm×210mm Rx, 40mm air gap magnetic coupler, and inductor/capacitor/capacitor-series (LCC-S) based decoupling compensation network. The experimental results show that output voltage varies in proportion to the mutual inductance of Tx and Rx. The measured efficiency is 89.5% to 94.5% under the voltage range of 155V to 220V during the 90mm misalignment.

INDEX TERMS Automated guided vehicle (AGV), compact magnetic coupler, inductive power transfer (IPT), output voltage fluctuation, size minimization.

I. INTRODUCTION

Recently, inductive power transfer (IPT) technology has attracted substantial attention in the scientific and industrial communities. With its inherent advantages, such as safety, flexibility, convenience and competence in the wet environment [1], [2], IPT technology is widely employed in electric vehicles (EVs) [3], medical devices [4], consumer electronics [5], and underwater power supplies [6]. As a special EV, automated guided vehicle (AGV) is productive and flexible, can run 24/7, and have become an essential technology in the modern logistics and warehousing industry [7], [8]. To achieve a higher degree of automation and avoid electrical sparks caused by frequently manual plug-in/out actions, IPT-based wireless charging technology is inevitably adopted, instead of plug-in charging.

The associate editor coordinating the review of this manuscript and approving it for publication was Chi-Seng Lam.

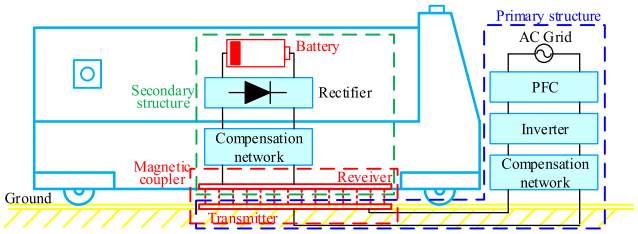

FIGURE 1. Structure of an IPT for AGV wireless charging system.

An IPT-based AGV wireless charging system is illustrated in Fig.1. The magnetic coupler composed of a transmitter (Tx) embedded under the ground, and a receiver (Rx) installed in the chassis of AGV, plays a crucial role in the wireless power transfer. Because of working indoors with relatively smooth road conditions, the chassis of AGV is usually several centimeters high [9]. However, the space of AGV's

chassis is relatively narrow, which presents a challenge to magnetic coupler design [10], [11]. Nowadays, to ensure stable wireless power transmission, the study on the magnetic coupler with more competitive anti-misalignment ability and minimized pad size is still a challenge.

To obtain the most appropriate magnetic coupler, various coil structures have been considered for AGV IPT application. And a scheme with the circular Tx and Rx is proposed in [11]. By optimal selection of coil turns, the maximum coil efficiency achieves 98.9% at 40mm air gap for 2.5kW power delivery. However, the coupling coefficient (k) of the magnetic coupler in [11] has an 8% reduction in 20mm misalignment distance, which raises the rigorous positioning accuracy requirement to AGV. Compared to the circular magnetic coupler, k of square coils of the same size has a stable performance [12]. Aiming at higher efficiency and better anti-misalignment ability, Choi et al. [13] propose a square coil with aluminum-plate-integrated structure. However, the output power decreases approximately by 60% as the lateral misalignment changes from 0mm to 50mm at a 50mm air gap.

The above-mentioned circular and square geometries belong to non-polarized couplers [14]. In practice, the fundamental flux path height of these pads is roughly proportional to one-quarter of the pad diameter [15]. And the misalignment range must be within one-third of the half-side or radius of the coils, beyond which the mutual inductance will decrease rapidly [12]. To improve both anti-misalignment ability and power transmission distance which are limited by miniaturized coil size, multi-coil polarized couplers like double-D (DD) pad [15], bipolar (BP) pad [16], and double-D quadrature (DDQ) pad [14] have been proposed. [15] presents a DD pad, whose fundamental flux path height is approximately half the length of the pad, and able to provide a higher k for the magnetic coupler. Moreover, the effective working area of a DD pad is five times greater than that of a circular pad with a similar size and cost. However, coupling null still exists when the lateral misalignment reaches 34% of the pad length, which leads the system sensitive to misalignment. In [14], a magnetic coupler with DD pad Tx and DDQ pad Rx is developed to avoid the coupling null point and expand the anti-misalignment distance. However, the quadrature (Q) pad uses more copper which consequently increases the cost and energy losses.

To achieve a greater tolerance against lateral misalignment and higher efficiency, the BP pad is presented for AGV application in [16]. Composed of two identical and partially overlapping rectangle coils, the BP pad can achieve mutual decoupling by adjusting the overlapping area of two Rx coils. And voltage superposition is realized via independent Rx coils in series. Although coupling null point could be avoided by the superposition of Rx coils, the overlapping area between two Rx coils depends on the decoupling requirement, which reduces design degrees of freedom, and cannot achieve the optimal output power design. Actually, this magnetic coupler presents nearly 50% output power ripples under 100mm lateral misalignment in the absence of a followed boost converter.

Nevertheless, it is indispensable for a BP pad to realize decoupling, even though the structure design might be limited. And the existence of undesirable cross-coupling results in detuning the resonant circuits that significantly reduces the power transfer capability and efficiency [17]. To make the BP pad structure achieve a more compact size for Rx and smoother output power under misalignment, the traditional mutual decoupling scheme of adjusting coils overlapping may be abandoned to obtain greater design freedom.

At present, except for the method of positioning the coils to nullify the overall mutual flux generated by neighboring Rx coil such as BP pad or DDQ pad, three predominant methods are used for reducing cross-coupling or completely decoupling between the Rx coils. And these decoupling methods include:

1) Displacing the Rx coils far from each other [18], [19], [20];

2) Using metal-insulator to reduce magnetic coupling [21];

3) Retuning the compensation networks of receivers by reflecting reactance [22], [23].

When the size of the Rx is significantly smaller than the Tx, the coils of the different receivers can be relatively far apart to reduce cross-coupling, as the structure of the four-phase Rx adopted by Cui et al. [18]. In order to prevent the coupling between the Rx coils from affecting the output characteristics of the IPT system, the Rx coils are connected by parallel-series-parallel (PSP), and only two phases without cross-coupling are working at any time. However, this method requires the size of Tx or Rx to be large enough, which poses design challenges due to the limited space of the AGV chassis. A mutual decoupling scheme based on magnetic shielding is proposed by [21], which uses an aluminum sheet and two ferrite cores to decouple the four-coil IPT system into two independent dual-coil sub-systems. And the common magnetic flux between the dual-coil sub-systems is shielded by the ferrite and aluminum on the magnetic field to achieve the purpose of decoupling. In this way, the mutual inductance of coils in the same class can be increased while the mutual inductance of coils in different classes is decreased. However, the fatal limitation of the magnetic decoupling scheme is that it is only applicable to the overlapped multi-receiving coils, but for the coils in the same plane, such as the BP pad or DDQ pad, this method is not effective. Retuning the compensation network of the two Rx coils is a reliable way to mitigate the cross-coupling effect. Still it also requires a real-time adaptive matching compensation network to handle the load and positional changes between Tx and Rx. A similar approach is used in [19] and [20], where additional reactance is inserted in the resonant tanks of the receiver structure to compensate for cross-coupling. However, the variation of the load or the mutual inductance between any of the three coils would require retuning the compensation network by

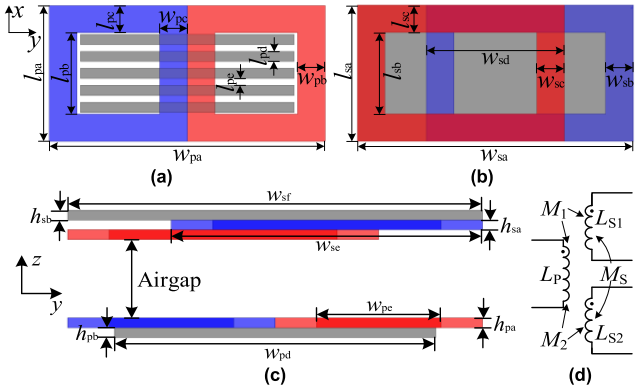

FIGURE 2. Structure of the proposed magnetic coupler. (a) Top view of the DD Tx. (b) Bottom view of the compact dual-coil Rx. (c) Side view of the proposed magnetic coupler. (d) Equivalent circuit model of the proposed magnetic coupler.

changing the capacitors used for matching [22]. This method is more meaningful in theory than in practice.

According to the above analysis, multi-coil Rx needs to be modeled again to acquire compact size and smooth output voltage characteristics during misalignment. In this paper, a DD Tx and a compact dual-coil Rx magnetic coupler collocation to independent decoupling method is applied to achieve size minimization, steadily and efficiently power transferring for AGV wireless charging system.

The rest of this paper is organized as follows. In Section II, the magnetic coupler, which is composed of a DD pad Tx and a compact dual-coil Rx is analyzed. Section III presents the impact on output characteristics by cross-coupling of compact dual-coil Rx. And an innovative mutual decoupling method for Rx decoupling is introduced in Section IV. In Section V, an experimental prototype is established to verify the magnetic coupler design and decoupling scheme. Finally, Section VI concludes this article.

II. ANALYSIS OF THE DD PAD TX AND COMPACT DUAL-COIL RX

To generate a sufficiently high magnetic field under the requirement of minimal Tx size, a DD pad is applied in this paper. Compared with other multi-coil polarized transmitters like BP pad or DDQ pad, the DD pad is wound by a single wire, which means the decoupling link caused by the multi-coil structure is omitted as well as the primary devices [24]. In order to obtain superior anti-misalignment ability, a dual-coil Rx consisting of two identical single-rectangle pads is analyzed. The proposed magnetic coupler and equivalent circuit model are shown in Fig.2, in which, w_{pa}, l_{pa}, w_{sa} and l_{sa} represent the width and length of Tx and Rx, respectively. And L_P is the self-inductances of the Tx, while L_{S1} and L_{S2} are the self-inductances of Rx. The mutual inductances between the Tx and dual-coil receiver are denoted as M_1 and M_2. Furthermore, M_S is the cross-coupling inductance between two Rx coils. And the equivalent mutual inductance

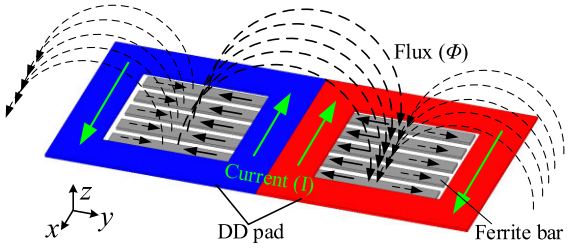

FIGURE 3. Flux pattern for DD Tx.

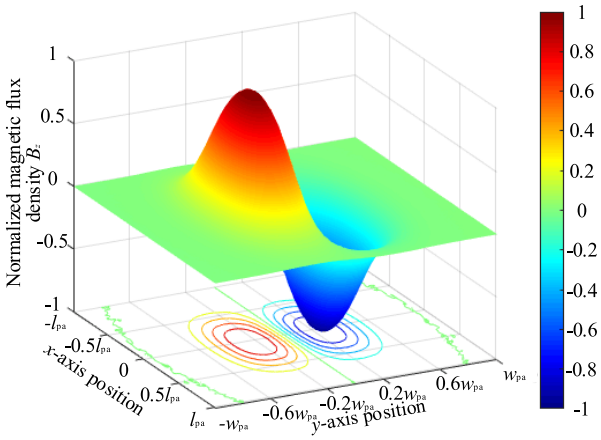

FIGURE 4. The simulation result of normalized magnetic flux density along the z-axis B_{zn} changing with the x-axis and y-axis position.

M_{eq} of the magnetic coupler could be expressed as:

$$M_{eq} = M_1 + M_2 \tag{1}$$

Usually, the windings of the coils along the outer sides are arranged in two-layer to ensure the transmission distance, while minimizing the size of the magnetic coupler by reducing the values of l_{pc}, l_{sc}, w_{pb} and w_{sb}.

In Fig. 3, the flux of DD pad Tx presents a parallel polarized feature and travels largely along the length of the pad, which allows the DD pad owns a higher fundamental flux path compared with the non-polarized coils. Before the design of the magnetic coupler, the magnetic field distribution which is generated by the Tx should be analyzed in the first place. As shown in Fig.3, the magnetic field generated by Tx can be decomposed into three dimensions along the x-axis, y-axis and

z-axis (indicated as B_x, B_y, and B_z), respectively. Since the directions of B_x, and B_y are parallel to the receiver plane, the magnetic field B_x and B_y have no influence on the mutual flux linkage passing through the Rx [24].

To analyze the magnetic field B_z on the Rx plane for the magnetic coupler without magnetic core quantitatively, finite element analysis (FEA) software ANSYS Maxwell has been used to simulate the field distribution. And the simulation result is shown in Fig. 4, and the normalized magnetic flux density along the z-axis B_{zn} is defined as:

$$B_{zn} = \frac{B_z}{\mathrm{MAX}(|B_z|)} \tag{2}$$

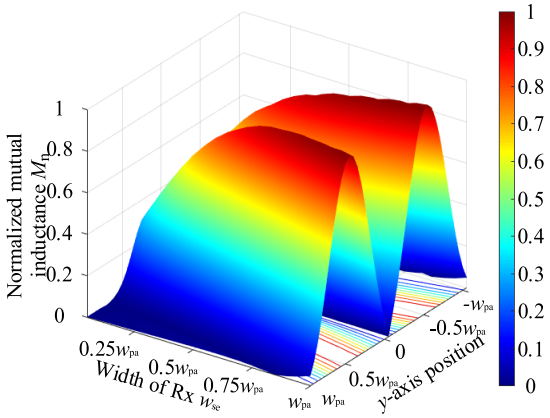

FIGURE 5. The simulation result of normalized mutual inductance varying with w_{se} and misalignment for DD Tx with single rectangle Rx.

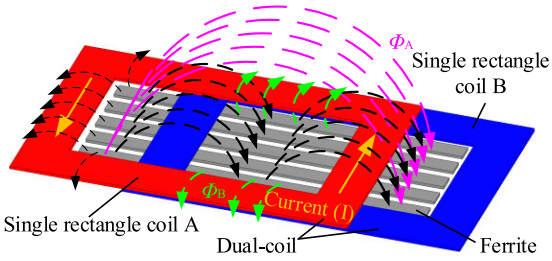

FIGURE 6. Flux pattern for the compact dual-coil Rx.

It can be obtained that the distribution of B_{zn} is symmetrical around the center of the origin. The mutual flux linkage passing through the single-rectangle pad could be calculated by:

$$\Phi = \int_S B_z(x, y)dS \tag{3}$$

where S indicates the effective flux area of the rectangle Rx, hence, the coupling null point will appear inevitably in the case when the center of the single-rectangle coil has zero misalignment along the y-axis from the origin.

Fig.5 shows the effect of the width of Rx relative to Tx on the mutual inductance of the magnetic coupler structure. And the normalized mutual inductance M_n between the DD Tx and single rectangle Rx is as follows:

$$M_n = \frac{M}{\mathrm{MAX}(M)} \tag{4}$$

where M represents the mutual inductance between the DD Tx and single rectangle Rx.

It should be noticed that the mutual inductance M of the magnetic coupler has no distinction on the positive and negative in number, as the difference in the direction of misalignment, the mutual inductance between the DD pad Tx and the single rectangle coil Rx is embodied in the difference of the dotted terminal. Actually, with the transposition of the y-axis misalignment, the dotted terminal of the magnetic coupler shifts. And it can be observed that the mutual inductance of DD pad Tx and single rectangle coil Rx increases rapidly

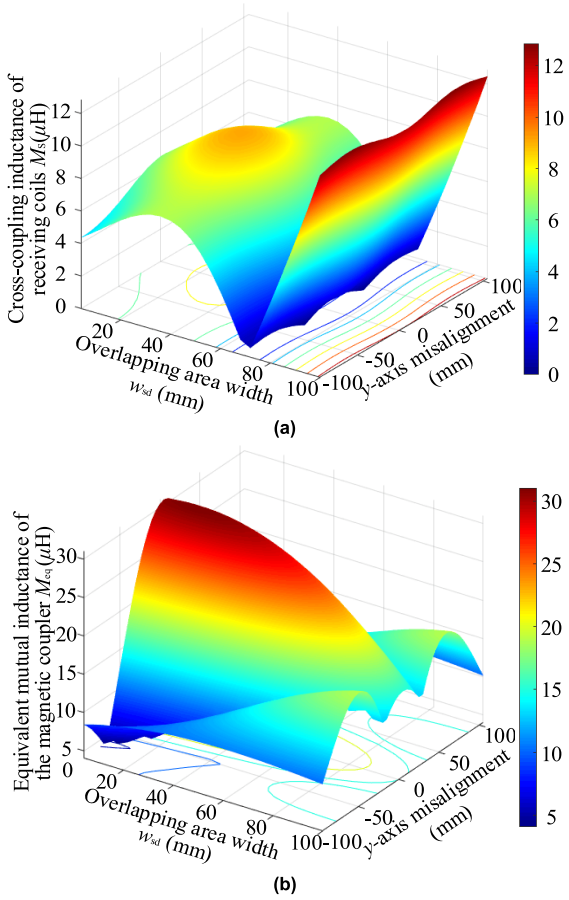

FIGURE 7. The simulation results of mutual inductance of the magnetic coupler. (a) M_s varying with w_{sd} and y-axis misalignment. (b) M_{eq} varying with w_{sd} and y-axis misalignment.

while $w_{sa} < 0.5w_{pa}$, and the growth of M starts to slow when $w_{sa} > 0.5w_{pa}$. Thus, the width of single-rectangle coil values from 0.5 to 0.7 w_{pa} is preferred. Obviously, the anti-misalignment ability of the magnetic coupler is strengthened with w_{se} growth. However, the coupling null point emerges when the rectangle Rx is aligned with DD pad Tx. To eliminate the coupling null point and improve the smoothness of M_{eq}, the design of multi-coil Rx plays a crucial role.

In general, according to the superposition theory, complex magnetic couplers such as BP pads, DDQ pads, or other compound pads design Rx could be piled up by fundamental pads [12], [25], and the proposed Rx has no exception. The flux pattern for compact dual-coil Rx is shown in Fig.6. While:

$$\Phi_A \neq \Phi_B \tag{5}$$

There is cross-coupling between the Rx coils. And the BP pad achieved decoupling by overlapping these two coils with specific overlapping areas to realize:

$$\Phi_A = \Phi_B \tag{6}$$

However, the fixed overlapping area significantly decreases dual-coil Rx's degree of freedom. In most

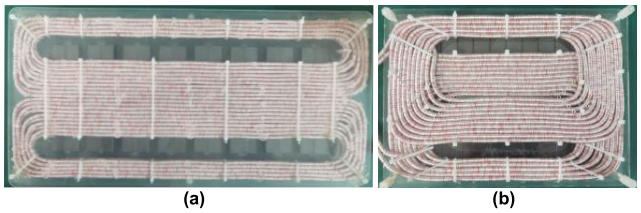

FIGURE 8. The physical picture of the magnetic coupler. (a) DD pad Tx. (b) Dual-coil Rx.

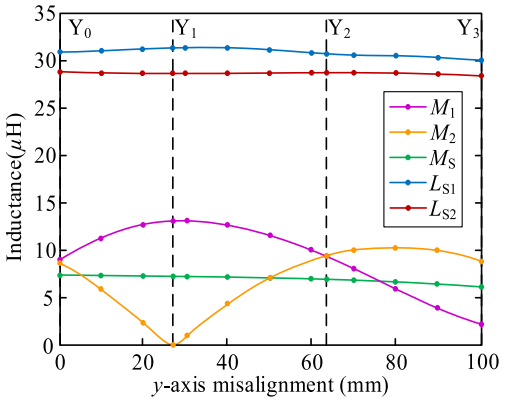

FIGURE 9. Measured self-inductances and mutual inductances of the magnetic coupler.

TABLE 1. Dimension parameters of the proposed magnetic coupler.

Parameter	Value	Parameter	Value	Parameter	Value
Air gap	40mm	w_{pa}	180mm	l_{sc}	44mm
N_F	8	w_{pb}	22mm	w_{sa}	150mm
N_S	10	w_{pc}	44mm	w_{sb}	22mm
N_P	10	w_{pd}	120mm	w_{sc}	44mm
l_{pa}	390mm	w_{pe}	24mm	w_{sd}	80mm
l_{pb}	346mm	h_{pa}	4.4mm	w_{se}	115mm
l_{pc}	22mm	h_{pb}	5mm	w_{sf}	150mm
l_{pd}	30mm	l_{sa}	210mm	h_{as}	4.4mm
l_{pe}	10mm	l_{sb}	122mm	h_{sb}	5mm

instances, the BP pad failed to implement the smoothest M_{eq} between Tx and Rx. To find the optimal M_{eq} for the magnetic coupler, a simulation is run to analyze the coupling characteristics of the magnetic coupler. Considering the AGV's relatively low chassis, the air gap of the magnetic coupler is determined to be 40mm. To acquire the sufficient height of magnetic field path, the Tx with the DD pad sized at $w_{pa} \times l_{pa} = 180\text{mm} \times 390\text{mm}$ is modeled, the number of ferrite bar N_F is set to 8, and the number of turns of Tx and Rx (N_P and N_S) is set to 10. Referring to Fig.5, to obtain adequate M_{eq} and anti-misalignment ability, the w_{sa} / w_{pa} is selected around 0.6. Thus, the single-rectangle pad size is chosen to $w_{se} \times l_{sa} = 115\text{mm} \times 210\text{mm}$. And l_{pa} is set larger than l_{sa} to acquire sufficient x-axis anti-misalignment

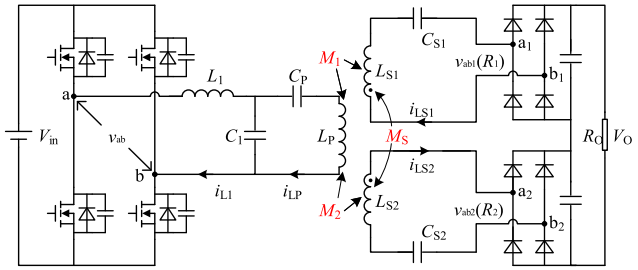

FIGURE 10. IPT charging system configuration.

ability (l_x). It can be expressed as:

$$l_x \approx \frac{l_{pa} - l_{sa}}{2} \tag{7}$$

As shown in Fig.7, with the increase of w_{sd}, the fluctuation of M_{eq} tends to be stable in the y-axis misalignment. However, while $w_{sd} > 80\text{mm}$, M_{eq} in the case of misalignment is less than

the maximum M_{eq}, which causes M_{eq} fluctuation to be larger. And while the overlapping area is constant, M_S fluctuates very little in misalignment, which could be almost negligible. In order to improve the anti-misalignment ability and the stability of M_{eq} during misalignment, the overlapping area is applied to make one Rx coil reaches the coupling highest point while the other coil is at the coupling null point. Moreover, the windings of the coils along the outer sides are arranged in two layers to reduce the size of the magnetic coupler further. The parameters of the magnetic coupler are listed in Table 1. And the magnetic coupler is constructed as shown in Fig.8.

From Fig.9, four special locations have been picked out for measurement. Y_0 is the position where Rx is exactly on top of Tx, and has no misalignment. Y_1 is the coupling peak point of receiving coil A and the coupling null point of receiving coil B, which, there is about 27mm y-axis misalignment distance. And it should be noted that the dotted terminal between the Tx and receiving coil B shifts while the y-axis misalignment goes through Y_1. While Rx is on Y_2, the mutual inductance of the two receiving coils is equal, and this point is about 63mm misalignment. Y_3 is the point at which Rx has a 100mm misalignment. And the variations of M_S, L_{S1}, and L_{S2} are within 1μH during the misalignment, the coupling maximum point of M_1 occurs at the same position as the coupling null point of M_2, which proves the feasibility of the proposed magnetic coupler.

III. ANALYSIS OF DD TX AND COMPACT DUAL-COIL RX BASED ON LCC-S COMPENSATION NETWORK

To improve the power factor of the IPT system and reduce reactive power loss, an inductor/capacitor/capacitor-series (LCC-S) compensation network [26], [27] is adopted in the proposed IPT system. With the constant current characteristic of the Tx coil as well as the constant voltage characteristic of output, the LCC-S compensation network allows

Tx to produce a stable magnetic field and simplify the Rx side [28], [29]. In order to achieve output voltage superposition for more power, the compact Rx coils are connected in series.

Fig.10 illustrates the proposed magnetic coupler with an LCC-S compensation network. The system consisted of a full bridge inverter on the primary side and two rectifiers on the secondary side, connected by a compensation inductance L_1, a parallel compensation capacitance C_1, and a series compensation capacitance C_P, a loosely coupled transformer composed of L_P, L_{S1}, and L_{S2}, and series compensation capacitances C_{S1}, C_{S2}. The DC voltage V_{in} and V_O are the corresponding input and output voltage. Where v_{ab}, v_{ab1}, and v_{ab2} are the midpoint voltages of the inverter and rectifiers, respectively. The DC load R_O could be equivalent to the sum of two AC loads of Rx circuits R_{eq}. And $R_{eq} = R_1 + R_2$, where R_1 and R_2 present the AC load of each Rx circuit loop.

Considering fundamental harmonic analysis (FHA), Fig. 10 can be simplified to a linear circuit and in which, the voltage/current variable, e.g., v_{ab}, v_{ab1}, v_{ab2}, i_{LP}, i_{L1}, i_{LS1} and i_{LS2}, their fundamental components could be written as $\dot{V}_{ab}$, $\dot{V}_{ab1}$, $\dot{V}_{ab2}$, $\dot{I}_{LP}$, $\dot{I}_{L1}$, $\dot{I}_{LS1}$, and $\dot{I}_{LS2}$ respectively. Similarly, V_{ab}, V_{ab1}, V_{ab2}, I_{LP}, I_{L1}, I_{LS1}, and I_{LS2} represent corresponding RMS value. The KVL equations of two Rx loops are established as follows:

$$\begin{cases} j\omega M_1 \dot{I}_{LP} = \left(j\omega L_{S1} + \frac{1}{j\omega C_{S1}} + R_1\right)\dot{I}_{LS1} + j\omega M_S \dot{I}_{LS2} \\ j\omega M_2 \dot{I}_{LP} = \left(j\omega L_{S2} + \frac{1}{j\omega C_{S2}} + R_2\right)\dot{I}_{LS1} + j\omega M_S \dot{I}_{LS1} \end{cases} \tag{8}$$

In the resonance state:

$$\begin{aligned} \omega &= \frac{1}{\sqrt{L_1 C_1}} = \frac{1}{\sqrt{(L_P - L_1)\, C_P}} \\ &= \frac{1}{\sqrt{L_{LS1} C_{LS1}}} = \frac{1}{\sqrt{L_{LS2} C_{LS2}}} \end{aligned} \tag{9}$$

where ω is the resonant angular frequency. When the cross-coupling exists between the Rx coils, the current of the Tx could be regarded as the excitation source, and the current of the two Rx coils are:

$$\begin{cases} \dot{I}_{LS1} &= \frac{j\omega M_1 R_2 + \omega^2 M_S M_2}{R_1 R_2 + \omega^2 M_S^2} \dot{I}_{LP} \\ \dot{I}_{LS2} &= \frac{j\omega M_2 R_1 + \omega^2 M_S M_1}{R_1 R_2 + \omega^2 M_S^2} \dot{I}_{LP} \end{cases} \tag{10}$$

Due to the series connection in the load circuit, $I_{LS1} = I_{LS2}$ in the case both Rx coils are working together, and it can be inferred:

$$\omega^2 M_2^2 R_1^2 + \omega^4 M_S^2 M_1^2 = \omega^2 M_1^2 R_2^2 + \omega^4 M_S^2 M_2^2 \tag{11}$$

From (9) to (11), the following equations are obtained:

$$\begin{cases} R_1 &= \frac{M_1^2 R_{eq} - \sqrt{\kappa}}{M_1^2 - M_2^2} \\ R_2 &= \frac{-M_2^2 R_{eq} + \sqrt{\kappa}}{M_1^2 - M_2^2} \end{cases}, \quad (M_1 \neq M_2)$$

$$\begin{cases} R_1 = \frac{1}{2} R_{eq} \\ R_2 = \frac{1}{2} R_{eq} \end{cases}, \quad (M_1 = M_2) \tag{12}$$

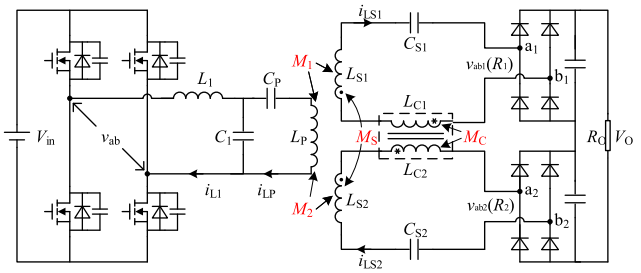

FIGURE 11. IPT charging system circuit topology with decoupling device.

where $\kappa = M_1^2 M_2^2 R_{eq}^2 + \omega^2 M_S^2 (M_1^2 - M_2^2)^2$, and the output power could be expressed:

$$\begin{cases} P_O = \frac{\delta}{1 + \frac{2M_1 M_2}{(M_1 - M_2)^2}\left(1 - \sqrt{\frac{M_1^2 M_2^2 R_O^2}{\kappa}}\right)}, & (M_1 \neq M_2) \\ P_O = \frac{\delta R_O^2}{R_O^2 + 4\omega^2 M_S^2}, & (M_1 = M_2) \end{cases} \tag{13}$$

where $\delta = (\omega M_1 + \omega M_2)^2 I_P^2 / R_O$. It can be concluded from (13) that the existence of cross-coupling will destroy the resonance condition of the IPT system. In the case of the same I_{LP} in the Rx, M_S inevitably reduces the output voltage as well as output power.

IV. DECOUPLING METHOD FOR THE IPT SYSTEM

According to the analysis in section III, the output performance of the system is greatly affected by M_S, so it is necessary to eliminate the cross-coupling by introducing the decoupling method. Distinguishing from the existing way, the decoupling method proposed in this article is to add an additional device between two receiving compensation networks, and counteract the mutual inductance between the Rx coils by generating opposite magnetic flux, so as to realize the decoupling. And the equivalent circuit is shown in Fig.11. As the decoupling devices, two lumped inductances L_{C1} and $L_{C2}$are integrated into one core, and the mutual inductance of L_{C1} and L_{C2} can be expressed as M_C. According to KVL, each secondary circuit loop equation could be expressed as:

$$\begin{cases} j\omega M_1 \dot{I}_{LP} = \left(j\omega L_{S1} + j\omega L_{C1} + \frac{1}{j\omega C_{S1}} + R_1\right)\dot{I}_{LS1} \\ \qquad\qquad + j\omega (M_S - M_C)\dot{I}_{LS2} \\ j\omega M_2 \dot{I}_{LP} = \left(j\omega L_{S2} + j\omega L_{C2} + \frac{1}{j\omega C_{S2}} + R_2\right)\dot{I}_{LS2} \\ \qquad\qquad + j\omega (M_S - M_C)\dot{I}_{LS1} \end{cases} \tag{14}$$

As seen from the (14), in the case of $M_C = M_S$, the term of equation $\dot{I}_{LS2}$ in receiving compensation network 1 will be eliminated, showing that L_{S1} receiving circuit will not be affected by the current in L_{S2} receiving circuit, so the same as the loop 2. Thus, the mutual decoupling of the two receiving circuit loops is achieved.

According to the proposed decoupling method, as M_C is equal to M_S, the value of the resonant capacitance C_{S1} and C_{S2} also needs to be re-matched to realize the resonance state

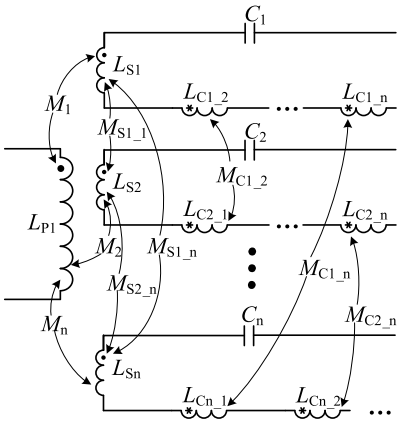

FIGURE 12. Proposed decoupling method for multi-coil decoupling.

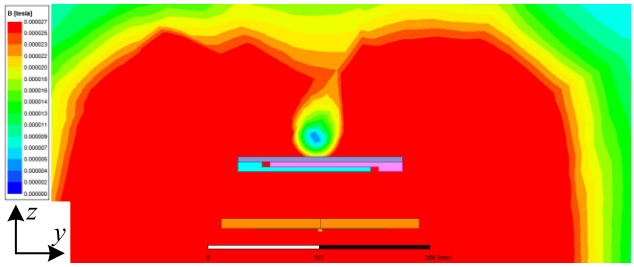

FIGURE 13. Distribution of leakage flux of the proposed wireless charging system.

of the IPT system. The conditions for the resonance of the two receiving circuit loops are as follows:

$$\omega = \frac{1}{\sqrt{L_1 C_1}} = \frac{1}{\sqrt{(L_P - L_1)\, C_P}} = \frac{1}{\sqrt{(L_{LS1} + L_{LC1}) C_{LS1}}} = \frac{1}{\sqrt{(L_{LS2} + L_{LC2}) C_{LS2}}} \tag{15}$$

With the Fourier transform, V_{ab} and R_{eq} can be expressed as:

$$V_{ab} = \frac{2\sqrt{2}}{\pi} V_{in} \tag{16}$$

$$R_{eq} = R_1 + R_2 = \frac{8}{\pi^2} R_O \tag{17}$$

The currents of the IPT system are obtained:

$$\begin{cases} \dot{I}_{L1} = \dfrac{M_{eq}^2 \dot{V}_{ab}}{L_1^2 R_{eq}}, & \dot{I}_{LP} = \dfrac{\dot{V}_{ab}}{\omega L_1} \\ \dot{I}_{LSi} = \dfrac{M_{eq}}{L_1 R_{eq}} \dot{V}_{ab}, & i = 1, 2 \end{cases} \tag{18}$$

In the case where the two receiving circuits are decoupled, the output voltage and output power can be expressed as:

$$V_O = \frac{M_{eq}}{L_1} V_{in} \tag{19}$$

$$P_O = \frac{M_{eq}^2 \cdot V_{in}^2}{L_1^2 \cdot R_O} \tag{20}$$

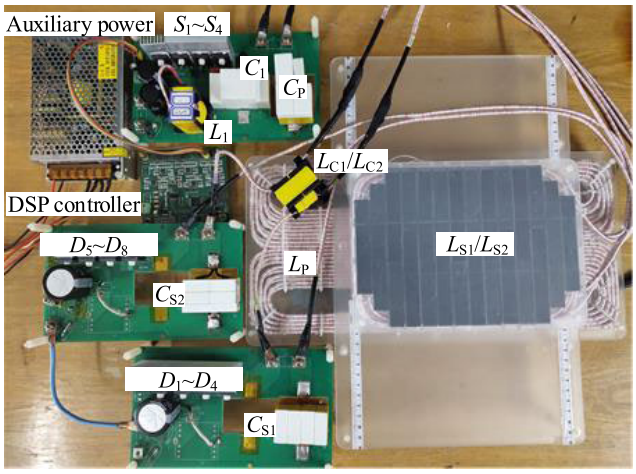

FIGURE 14. Experimental prototype.

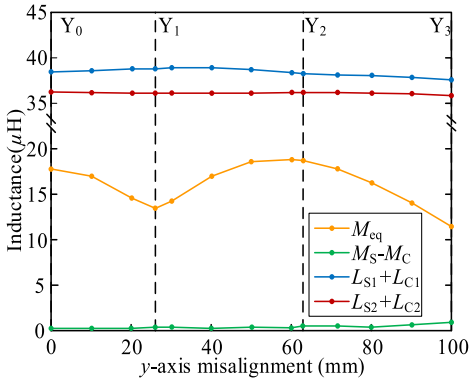

FIGURE 15. Measured self-inductances and mutual inductances after decoupling.

As shown in (18) to (20), the current of Tx and Rx, output voltage V_O, and output power P_O are no longer affected by M_S, which proves the effectiveness of the decoupling method.

On account the combination of the dual-coil receivers and decoupling device can be equivalent to the uncoupled dual-coil receivers, the presented decoupling method is appropriate for any compensation network. Furthermore, the proposed decoupling method is also suitable for multi-coil structures both in Tx and Rx, as shown in Fig. 12. For the multi-coil situation, the multiple decoupling devices can be integrated into one or a few decoupling devices to improve the power density, which is unable to be achieved by traditional capacitive decoupling methods. At the same time, the decoupling device is incorporated into the compensation network to meet the condition of the receiving coils separated by a large distance.

Since the DD Tx is assumed to be embedded in the road, and the leakage flux intensity of DD Tx in the y-axis misalignment direction on the road is simulated and presented in Fig. 13. Compared with the leakage flux of 27 μT in ICNIRP2010 standard, the minimum safe distance of proposed magnetic coupler is about 150mm.

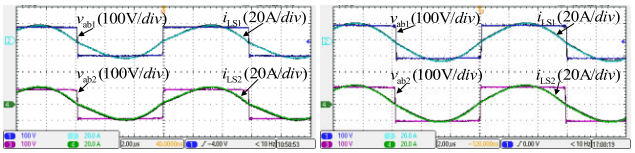

FIGURE 16. Rx waveforms at the Y_0 test point. (a) Coupled. (b) Decoupled.

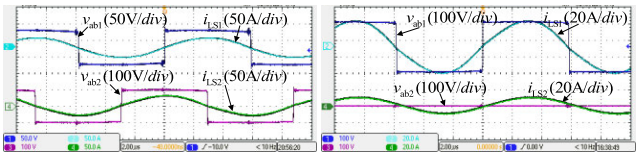

FIGURE 17. Rx waveforms at the Y_1 test point. (a) Coupled. (b) Decoupled.

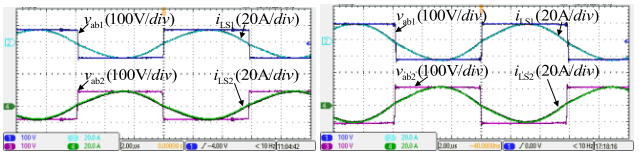

FIGURE 18. Rx waveforms at the Y_2 test point. (a) Coupled. (b) Decoupled.

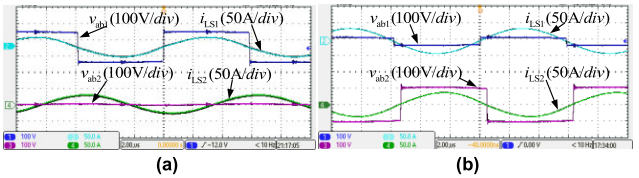

FIGURE 19. Rx waveforms at the Y_3 test point. (a) Coupled. (b) Decoupled.

TABLE 2. System parameters before decoupling.

Parameter	Value	Parameter	Value	Parameter	Value
V_{in}	400 V	C_P	42.9 nF	L_{S2}	28.7 μH
L_1	33.4 μH	f_s	85kHz	C_{S1}	114 nF
L_P	115 μH	L_{S1}	30.8 μH	C_{S2}	122 nF
C_1	105 nF				

TABLE 3. System parameters of receiver after decoupling.

Parameter	Value	Parameter	Value	Parameter	Value
L_{S1}	30.8 μH	L_{C1}	8.7 μH	C_{S1}	88 nF
L_{S2}	28.7 μH	L_{C2}	8.8 μH	C_{S2}	93 nF

V. EXPERIMENT RESULTS

To verify the proposed magnetic coupler design and mutual decoupling solution, an experimental prototype based on the proposed magnetic coupler is established, as shown in Fig. 14.

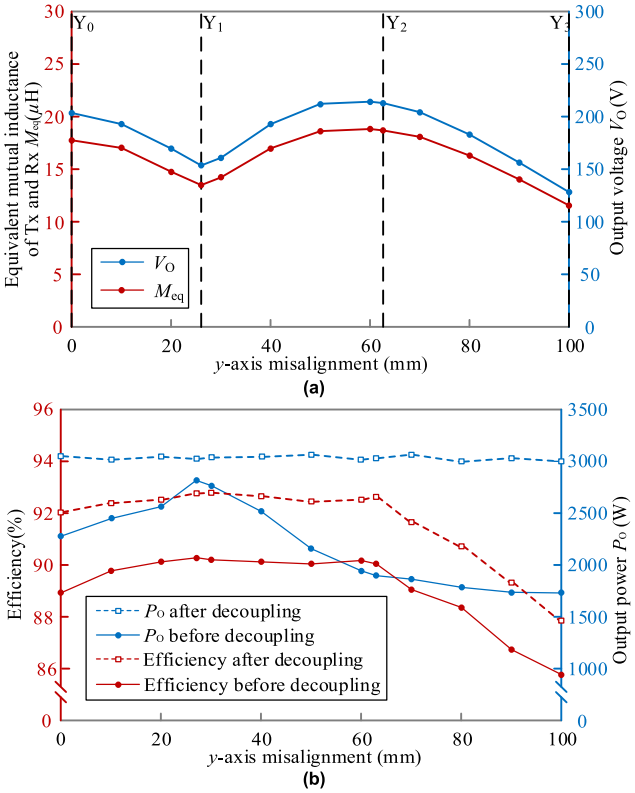

FIGURE 20. Output characteristics of the IPT system. (a) Measured equivalent mutual inductance and output voltage. (b) System efficiency and output power with y-axis misalignment.

In addition, the measured self-inductances and mutual inductances after decoupling are demonstrated in Fig. 15, in which the cross-coupling M_S could be eliminated completely by M_C. The specific parameters of the experimental prototype are given in Table 2 and Table 3. In order to reduce the inductive reactance of the receivers, the decoupling device is wound into a closely coupled structure similar to a typical transformer.

$Y_0 \sim Y_3$ are the specific test points for the IPT system's output characteristics, and the waveforms of AC output voltages, as well as each Rx coil current before and after decoupling, are shown in Fig. 16$\sim$19, and the experiments are arranged as follows:

1). In order to compare the output characteristics of the IPT system before and after decoupling, M_C is replaced with a series compensation capacitance while the load R_O is keeping constant to test the output characteristics under cross-coupling in four different positions along the y-axis.

2). To illustrate the performance of the decoupling solution, in this decoupling experiment, the output power P_O is kept at 3kW by adjusting the resistance R_O under the disturbance of misalignment.

Y_0 is the point where the Rx has no misalignment against Tx, and M_1 is equal to M_2, as shown in Fig.16, the waveforms of v_{ab1} and v_{ab2} are in the same phase both decoupled and coupled. And the circuit works in resonance.

TABLE 4. Comparison of magnetic couplers for the AGV IPT system.

References	This work	[10]	[11]	[13]	[16]
Air gap/mm	40	25	40	50	30
Tx type	DD	Square	Circular	Square	Four-conductor track
Rx type	Compact dual coils	Square	Circular	Square	BP
Width of Rx (w_{sa})/mm	150	220	300	250	300
Length of Rx (l_{sa})/mm	210	220	300	250	300
Anti-misalignment ability/(mm)	±90	/	/	±50	±200
Rx voltage fluctuation	±17.3%	/	/	/	±40%
Frequency/kHz	85	85	138	85	10
Output power/kW	3	1.8	2.5	1	0.3
Peak efficiency	94.5%	87.7%	/	96%	/

However, while the Rx is misalignment, M_1 and M_2 are going to unbalance, which means the resonance state of the circuit is broken.

Fig. 17(a) shows that v_{ab2} (i_{LS2}) have 90° phase in advance compared with v_{ab1} (i_{LS1}). This is because Y_1 is the coupling null point of Rx coil L_{S2}, and v_{ab2} is generated by the i_{LS1} through cross-coupling M_S between the Rx coils. After decoupling, the voltage induced in M_C and the voltage induced in M_S eliminated each other, so the v_{ab2} comes to zero. According to Fig.18, Y_2 is the point where M_1 is equal to M_2. However, v_{ab1} and i_{LS1} have a 180° phase differences compared with v_{ab2} and i_{LS2}. This is because the magnetic flux Φ flowing through the Rx coil L_{S2} at Y_2 is reversed from that at Y_0, resulting in the dotted terminal changing of the coil L_{S2}, so as the decoupling device.

As it can be obtained in Fig.19, the resonance characteristics of the IPT system are completely disturbed before decoupling. However, v_{ab1} and i_{LS1} start to have teeny incomplete reversal phase differences compared with v_{ab2} and i_{LS2} after decoupling, which is caused by the fluctuation of L_{S1}, L_{S2}, and M_S at a sufficiently large misalignment distance.

As last, the output performance of the IPT system are shown in Fig.20. And Fig.20(a) shows the output voltage and the equivalent mutual inductance varying with the y-axis misalignment. As it could be obtained that M_{eq} varies between 14.1μH to 19.5μH in 0∼90mm y-axis misalignment, while V_O ranges from 155V to 220V. Fig.19(a) illustrates the fluctuations of V_O and M_{eq} are relatively stable and proportional to each other, which indicates that the coupling between the receivers is neutralized, thus verifying the effectiveness of the decoupling method and magnetic coupler design. As shown in Fig.20(b), the maximum and minimum efficiency of the system when the output power is 3kW are 94.5% and 89.5% in the designed misalignment range. In contrast, the output power and efficiency of the system are relatively lower with the same load condition when the Rx coils are not decoupled. Thus, proving the improvement of the power and efficiency of the IPT system by this decoupling method.

In comparison with previously published magnetic couplers in Table 4, the proposed compact magnetic coupler can achieve relatively high peak efficiency and output power with reduced Rx size. This will not only meet the charging performance, but also significantly reduce the occupancy of the AGV chassis space by the IPT system. While compared with the self-decoupling coils, the proposed magnetic coupler accompanying with decoupling device has a more compact size for the receiver, and shows higher design freedom for the magnetic coupler. In addition, the proposed decoupling scheme is more flexible and has higher power density than the schemes in [18], [19], [20], and [21], and it is simpler in control when compared with [22] and [23].

VI. CONCLUSION

A magnetic coupler consists of a DD pad Tx and a compact dual-coil Rx, which pursues size and output power fluctuation minimization is proposed in this paper. The conclusion could be obtained through detailed magnetic circuit analysis and FEA simulation: By overlapping the Rx coils in a specific area, in which one coil reaches the coupling highest point, the other coil is at the coupling null point, thus, realizing stable wireless power transmission during the misalignment. And while the rectangle coils of the dual-coil Rx reach 0.5∼0.7 times of DD Tx's width, the magnetic coupler could achieve sufficient coupling. Moreover, to achieve mutual decoupling of Rx dual-coil, a decoupling method has been proposed, which uses two lumped inductors possessing the same mutual inductance as the Rx coils. Based on the proposed magnetic coupler design and decoupling method, an LCC-S compensated IPT system is established. The experimental results show that V_O varies in proportion to mutual inductance M_{eq}. The efficiency and output voltage range of 89.5% to 94.5% and 155V to 220V during the 90mm y-axis misalignment, while the output power is 3kW, shows the effectiveness of the decoupling method and magnetic coupler design.

REFERENCES

[1] X. Zhang, F. Liu, and T. Mei, "Multifrequency phase-shifted control for multiphase multiload MCR WPT system to achieve targeted power distribution and high misalignment tolerance," *IEEE Trans. Power Electron.*, vol. 36, no. 1, pp. 991–1003, Jan. 2021.

[2] Y. Yao, Y. Wang, X. Liu, F. Lin, and D. Xu, "A novel parameter tuning method for a double-sided LCL compensated WPT system with better comprehensive performance," *IEEE Trans. Power Electron.*, vol. 33, no. 10, pp. 8525–8536, Oct. 2018.

[3] S. Lukic and Z. Pantic, "Cutting the cord: Static and dynamic inductive wireless charging of electric vehicles," *IEEE Electrific. Mag.*, vol. 1, no. 1, pp. 57–64, Sep. 2013.

[4] V. Valente, C. Eder, N. Donaldson, and A. Demosthenous, "A high-power CMOS class-D amplifier for inductive-link medical transmitters," *IEEE Trans. Power Electron.*, vol. 30, no. 8, pp. 4477–4488, Aug. 2015.

[5] J. Kim, H.-C. Son, D.-H. Kim, and Y.-J. Park, "Optimal design of a wireless power transfer system with multiple self-resonators for an LED TV," *IEEE Trans. Consum. Electron.*, vol. 58, no. 3, pp. 775–780, Aug. 2012.

[6] H. Fukuda, N. Kobayashi, K. Shizuno, S. Yoshida, M. Tanomura, and Y. Hama, "New concept of an electromagnetic usage for contactless communication and power transmission in the ocean," in *Proc. IEEE Int. Underwater Technol. Symp. (UT)*, Mar. 2013, pp. 1–4.
[7] D. Wang, C. Fu, X. Bei, and Q. Zhao, "A reconfigurable half-bridge compensation topology-based WPT system with constant current and constant voltage outputs," *IEEE Trans. Circuits Syst. II, Exp. Briefs*, vol. 70, no. 1, pp. 256–260, Jan. 2023.
[8] F. Lu, Y. Zhang, H. Zhang, C. Zhu, L. Diao, M. Gong, W. Zhang, and C. Mi, "A low-voltage and high-current inductive power transfer system with low harmonics for automatic guided vehicles," *IEEE Trans. Veh. Technol.*, vol. 68, no. 4, pp. 3351–3360, Apr. 2019.
[9] B. Yang, Y. Lu, Y. Peng, S. He, Y. Chen, Z. He, R. Mai, and Z. Wang, "Analysis and design of a T/S compensated IPT system for AGV maintaining stable output current versus air gap and load variations," *IEEE Trans. Power Electron.*, vol. 37, no. 5, pp. 6217–6228, May 2022.
[10] F. Lu, H. Zhang, C. Zhu, L. Diao, M. Gong, W. Zhang, and C. C. Mi, "A tightly coupled inductive power transfer system for low-voltage and high-current charging of automatic guided vehicles," *IEEE Trans. Ind. Electron.*, vol. 66, no. 9, pp. 6867–6875, Sep. 2019.
[11] E. S. Lee and S. H. Han, "2-D thin coil designs of IPT for wireless charging of automated guided vehicles," *IEEE J. Emerg. Sel. Topics Power Electron.*, vol. 10, no. 2, pp. 2629–2644, Apr. 2022.
[12] Z. Luo and X. Wei, "Analysis of square and circular planar spiral coils in wireless power transfer system for electric vehicles," *IEEE Trans. Ind. Electron.*, vol. 65, no. 1, pp. 331–341, Jan. 2018.
[13] J. S. Choi, S. Y. Jeong, B. G. Choi, S.-T. Ryu, C. T. Rim, and Y.-S. Kim, "Air-gap-insensitive IPT pad with ferromagnetic and conductive plates," *IEEE Trans. Power Electron.*, vol. 35, no. 8, pp. 7863–7872, Aug. 2020.
[14] S. Bandyopadhyay, P. Venugopal, J. Dong, and P. Bauer, "Comparison of magnetic couplers for IPT-based EV charging using multi-objective optimization," *IEEE Trans. Veh. Technol.*, vol. 68, no. 6, pp. 5416–5429, Jun. 2019.
[15] M. Budhia, J. T. Boys, G. A. Covic, and C.-Y. Huang, "Development of a single-sided flux magnetic coupler for electric vehicle IPT charging systems," *IEEE Trans. Ind. Electron.*, vol. 60, no. 1, pp. 318–328, Jan. 2013.
[16] A. Zaheer, G. A. Covic, and D. Kacprzak, "A bipolar pad in a 10-kHz 300-W distributed IPT system for AGV applications," *IEEE Trans. Ind. Electron.*, vol. 61, no. 7, pp. 3288–3301, Jul. 2014.
[17] D. Ahn and S. Hong, "Effect of coupling between multiple transmitters or multiple receivers on wireless power transfer," *IEEE Trans. Ind. Electron.*, vol. 60, no. 7, pp. 2602–2613, Jul. 2013.
[18] S. Cui, Z. Wang, S. Han, and C. Zhu, "Analysis and design of multiphase receiver with reduction of output fluctuation for EV dynamic wireless charging system," *IEEE Trans. Power Electron.*, vol. 34, no. 5, pp. 4112–4124, May 2019.
[19] B. L. Cannon, J. F. Hoburg, D. D. Stancil, and S. C. Goldstein, "Magnetic resonant coupling as a potential means for wireless power transfer to multiple small receivers," *IEEE Trans. Power Electron.*, vol. 24, no. 7, pp. 1819–1825, Jul. 2009.
[20] J. J. Casanova, Z. N. Low, and J. Lin, "A loosely coupled planar wireless power system for multiple receivers," *IEEE Trans. Ind. Electron.*, vol. 56, no. 8, pp. 3060–3068, Aug. 2009.
[21] W. Chen, H. Li, and W. Lu, "Decoupling design of multi-coil wireless power transfer system with metal insulator," in *Proc. IEEE PELS Workshop Emerg. Technol., Wireless Power Transf. (WoW)*, May 2017, pp. 30–33.
[22] M. Fu, T. Zhang, P. C.-K. Luk, X. Zhu, and C. Ma, "Compensation of cross coupling in multiple-receiver wireless power transfer systems," *IEEE Trans. Ind. Informat.*, vol. 12, no. 2, pp. 474–482, Apr. 2016.
[23] G. Monti, W. Che, Q. Wang, A. Costanzo, M. Dionigi, F. Mastri, M. Mongiardo, R. Perfetti, L. Tarricone, and Y. Chang, "Wireless power transfer with three-ports networks: Optimal analytical solutions," *IEEE Trans. Circuits Syst. I, Reg. Papers, Reg. Papers*, vol. 64, no. 2, pp. 494–503, Feb. 2017.
[24] A. Zaheer, H. Hao, G. A. Covic, and D. Kacprzak, "Investigation of multiple decoupled coil primary pad topologies in lumped IPT systems for interoperable electric vehicle charging," *IEEE Trans. Power Electron.*, vol. 30, no. 4, pp. 1937–1955, Apr. 2015.
[25] R. Oliveira and P. Lehn, "An improved mutual inductance electromagnetic model for inductive power transfer systems under misalignment conditions," *IEEE Trans. Veh. Technol.*, vol. 69, no. 6, pp. 6079–6093, Jun. 2020.
[26] X. Gao, S. Dong, S. Cui, and C. Zhu, "Unbalanced reflected impedances and compensation of TS dynamic wireless charging system," *IEEE Trans. Ind. Electron.*, vol. 68, no. 11, pp. 10378–10387, Nov. 2021.
[27] C. Jiang, K. T. Chau, W. Liu, C. Liu, W. Han, and W. H. Lam, "An LCC-compensated multiple-frequency wireless motor system," *IEEE Trans. Ind. Informat.*, vol. 15, no. 11, pp. 6023–6034, Nov. 2019.
[28] X. Wang, J. Xu, H. Ma, and P. Yang, "A high efficiency LCC-S compensated WPT system with dual decoupled receive coils and cascaded PWM regulator," *IEEE Trans. Circuits Syst. II, Exp. Briefs*, vol. 67, no. 12, pp. 3142–3146, Dec. 2020.
[29] D. Wang, C. Fu, Q. Zhao, and T. Hu, "A PSO-based optimization design of W-type noncontact transformer for stable power transfer in DWPT system," *IEEE Trans. Ind. Appl.*, vol. 58, no. 1, pp. 1211–1221, Jan. 2022.

CHAOWEI FU (Member, IEEE) received the B.S. degree in electrical engineering and automation from Yanshan University, Hebei, China, in 2019, where he is currently pursuing the M.S. degree in electrical engineering.

He worked as a Design Engineer with SIEMENS Circuit Protection System Ltd., Shanghai, China, in 2019. His current research interests include wireless power transfer and high-frequency switching mode converter.

DEYU WANG (Member, IEEE) received the M.S. and Ph.D. degrees from the School of Electrical Engineering, Yanshan University, Qinhuangdao, China, in 2005 and 2009, respectively.

Since 2015, he has been an Associate Professor with the School of Electrical Engineering, Yanshan University. His research interests include wireless power transfer technology, high-frequency switching mode converter, and solid-state pulsed power application.

QINGLIN ZHAO received the M.S. and Ph.D. degrees from the School of Electrical Engineering, Yanshan University, Qinhuangdao, China, in 2003 and 2007, respectively.

He has been a Professor with the School of Electrical Engineering, Yanshan University, since 2010. His research interests include wireless power transfer technology, high-frequency switching mode converter, and control of grid-connected inverters.